ARMA 14-7514

Estimating Seismic Energy Release and Surface Area Generation: Implications for Interpreting Hydraulic Fracture Behavior

Cochrane, A., Urbancic, T.I. and Baig, A.M.

Engineering Seismology Group, Kingston, ON, Canada

Copyright 2014 ARMA, American Rock Mechanics Association

This paper was prepared for presentation at the 48th US Rock Mechanics / Geomechanics Symposium held in Minneapolis, MN, USA, 1-4 June 2014.

This paper was selected for presentation at the symposium by an ARMA Technical Program Committee based on a technical and critical review of the paper by a minimum of two technical reviewers. The material, as presented, does not necessarily reflect any position of ARMA, its officers, or members. Electronic reproduction, distribution, or storage of any part of this paper for commercial purposes without the written consent of ARMA is prohibited. Permission to reproduce in print is restricted to an abstract of not more than 200 words; illustrations may not be copied. The abstract must contain conspicuous acknowledgement of where and by whom the paper was presented.

ABSTRACT: During hydraulic fracture stimulations in shale, the activation of pre-existing fractures plays an important role in the development of the discrete fracture network. Understanding the behavior of the fracture network allows for the potential of incorporating the observed fracture network into reservoir models necessitating the identification of fracture behavior over a wide magnitude scale -3 < M < +3. Here, we discuss seismic events that were recorded by a multi-array multi-level network consisting of high frequency geophones located near the reservoir and arrays of accelerometers and low-frequency geophones deployed near the surface. The hybrid system captures a larger bandwidth, allowing for the integrated analysis of the source signal at various scales. Comparatively speaking, our observations suggest that the larger scale events identified on the near-surface network contribute upwards of 80% of the overall seismic budget or seismic energy release associated with the stimulation process. Additionally, these events accounted for a further 11,870 m^2 of activated fracture surface area, approximately 10,295 m^2 more than would have been estimated from the downhole array alone. Overall, the identification of the actual discrete fracture network over many size scales allows for a better understanding of the fracturing processes associated with stimulations.

1. INTRODUCTION

Hydraulic fracturing in naturally fractured reservoirs is known to generate seismicity due to the interaction of injected fluids with the pre-existing fracture network. Typically, the observed moment magnitudes for such operations are small, usually with Mw < 0. To map the seismicity during these injections, geophones (utilizing 15 Hz) are typically deployed in arrays in nearby wells. From such configurations information on the relative stimulation volumes and overall fracture dimensions can be obtained. However, the ubiquity of these high-frequency instruments has profound implications for the reliability of magnitude estimates for the largest events associated with these treatments. To address this concern, accelerometers and lower-frequency geophones along can be installed close to surface to characterize events over a wider magnitude band. Furthermore, these sensors can be combined with the high-frequency downhole geophones to monitor (hybrid sensor network) the full bandwidth of activity that can occur during fracture stimulation programs.

Recently, we have had the opportunity to supplement traditional downhole recording utilizing high frequency 3C 15 Hz sensors with a sparse eight station near surface network consisting of low frequency force balance accelerometers (>0.1Hz) and 4.5Hz geophones associated with hydraulic fracture stimulations in an unconventional shale play in North America (Figure 1). During the stimulation, a total of 4500 events were recorded on the downhole array situated close to the reservoir, ranging in magnitude from M-1 to M-2.6. The near surface network recorded a total of 28 events ranging from M-0.4 to M1.4; these events were also recorded on the downhole array, however the downhole signals exhibited magnitude saturation affects, which on average, resulted in underestimates of magnitude upwards of M-1.8 (Figure 2).

Significant to the study was the assessment of seismic energy release, which showed that the larger magnitude events detected with the near surface network accounted for a full 83% of the total seismic energy released during the stimulations. Additionally, these events accounted for a further 11,870 m^2 of activated fracture surface area, approximately 10,295 m^2 more than would have been estimated from the downhole array alone. Overall, the additional surface area as derived from the near

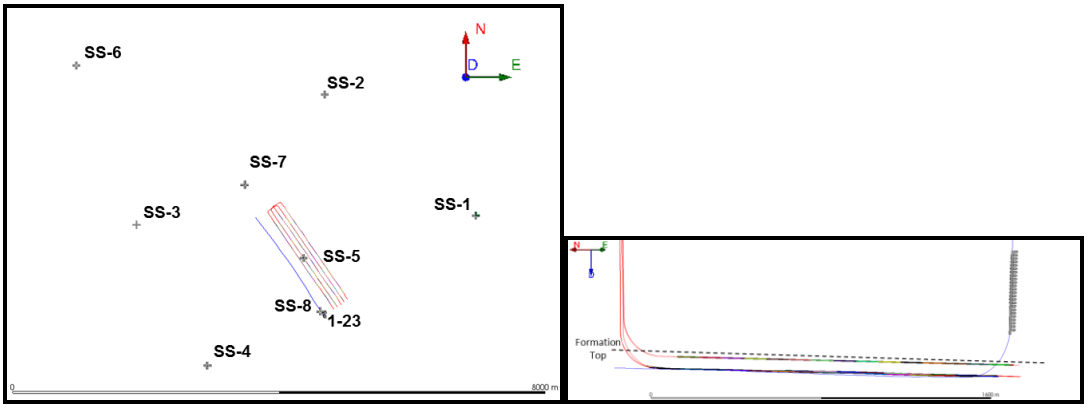

Figure 1. Plan (left) and depth (right) views of the treatment wells and monitoring geometry for the hydraulic stimulation discussed. A combination of surface stations (SS 1-8) consisting of force-balanced accelerometers and 4.5 Hz geophones and a downhole array comprised of 15 Hz elements were used to monitor the completion of the pad.

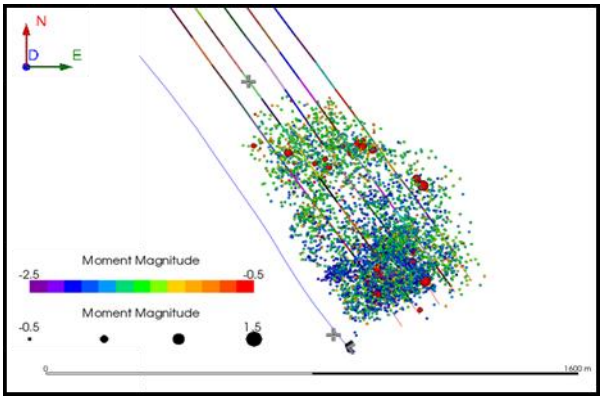

Figure 2. Events detected during the hydraulic fracture completion include several larger magnitude (red) events with signals that are strong enough to be detected on the surface network.

surface network accounts for <1% of all the recorded events but adds an additional 4% to the total liberated surface area when combined with the surface area generated by the 4500 events recorded downhole.

The effectiveness of the stimulation was easily evaluated through this monitoring program. The microseismic events could be used to identify growth from the lower to upper horizon with different pressure rates. The occurrences of larger magnitude events appeared to precede pressure increases in the program, suggesting that larger structures were activated as a result of the injection program even before pressures were increased. This was further exemplified by the inversion results for the M>0 events, which were dominated by shear failures associated with consistent fracture orientations in alignment with the regional stress field. Interestingly, a small rotation in the principal stresses is apparent resulting from the stimulation program. These observed process sets the foundation to better control and understand hydraulic fracture stimulation programs.

2. MAGNITUDE SATURATION

Moment magnitude (Mw) is a parameter that involves characterization of the low-frequency spectrum of the seismic or microseismic event. Often, when calculating the moment magnitudes over a large network of stations, the estimates from each station are averaged together, with some weights that can be applied to account for the instrument type or a number of other factors (e.g., attenuation). However, to fully examine how the heterogeneous sensor distribution is beneficial, we do not average the magnitudes in this fashion, but rather account for each instrument type separately. Hanks and Kanamori [1] stipulate how to calculate moment magnitude from seismic moment, which itself is measured from the long-period spectral amplitudes of the displacement spectrum (see also [2], for an overview of these calculations as applied to microseismic data) corrected for focal mechanism, source and site conditions, and geometrical spreading [3]. This low-frequency plateau is a feature of many source models [3, 4] that characterize the spectrum by the long-period level, corner frequency, and attenuation quality factor. From these quantities assessed from the displacement spectrum, the source parameters like moment, energy, source radius, stress drop, etc. are calculated.

In Figure 3, we show an example fit of a Brune spectrum to an event with Mw=2.3 [3]. This example features the spectra of the P waves as seen on all three of the sensor types that we discuss: an FBA; a 4.5 Hz geophone; and a 15 Hz geophone. The sensors shown are all associated with the same observation well, with the 4.5 Hz and 15 Hz geophone deployed downhole and the FBA on the surface, proximal to the well. A constant attenuation factor is applied to all of the spectra, but the influence of Q is to attenuate the high frequencies preferentially and does not affect necessarily the estimates of the long-period plateau in this example. This figure illustrates how the short-period stations (the geophones) underestimate the moment magnitudes of this large event; only the FBA accurately recovers the magnitude of Mw1.8, the other stations show saturation around Mw=1.8 and Mw=0.8. This depletion of low frequencies in the geophone records can also be observed by the breakdown of the noise signal around the natural period

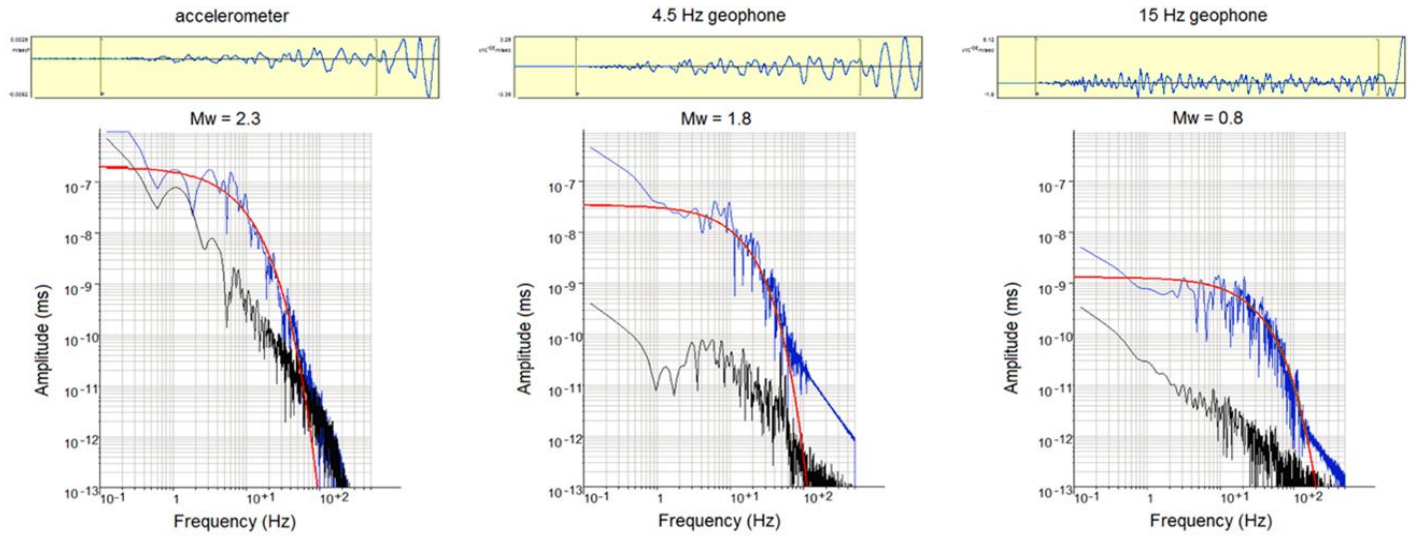

Figure 3. An example of magnitude saturation recorded from a site where the same event was recorded on a force-balance accelerometer (left), a 4.5 Hz geophone (center) and a 15 Hz geophone (right). The magnitude 2.3 event is faithfully recorded on the force-balance accelerometer, but the magnitude is understated by 0.5 and 1.5 magnitude units on the 4.5 Hz and 15 Hz geophones, respectively

of the instruments which is not observed at the FBA record.

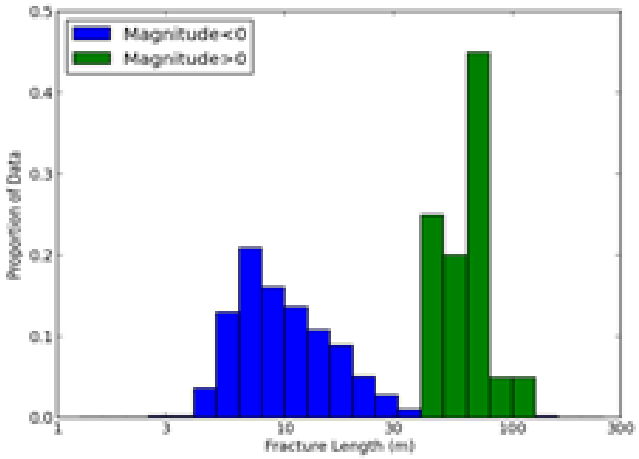

Figure 4. Histograms showing the relative proportion of the surface-recorded events' fracture radii (green) versus the downhole-recorded events (blue).

3. HYBRID PROCESSING

The addition of the lower-frequency sensors on or near the surface greatly aids in the correct determination of magnitudes and other source parameters, such as source dimensions and energy and stress release parameters. However, in the processing of these events, the locations are solely determined from the downhole array, because these sensors are closest to the source. The addition of the 4.5 Hz geophones and force balance accelerometers allows for the accurate calculation of the larger magnitude events depicted in figure 2. In figure 4, we show histograms of the source radii for the dataset showing how the addition of the near-surface sensors is able to access another size scale of fractures activated in the reservoir. The fracture length is determined from the Brune model [3] of a penny-shaped crack from measuring the corner frequency.

The addition of these length scales is critical for estimating the power law distribution controlling the fracture length distribution used in reservoir simulations [5]. The microseismic scale in general fills the gap in the sampling of fracture lengths in the reservoir between what can be observed in outcrop and core (centimeters to meters) to what can be observed and interpreted in seismic data volumes (hundreds of meters).

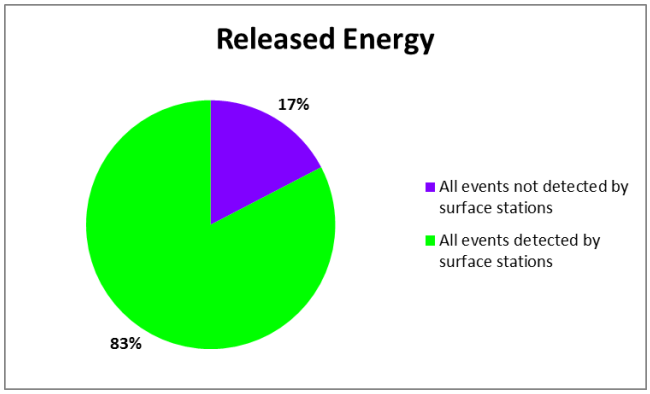

Figure 5. The energy radiated from the 28 events recorded on the surface stations comprise over 80% of total the energy from the 4500 events recorded over the course of the completion.

4. STIMULATION EFFECTIVENESS

The microseismicity outlined growth through the treatment formation and delineated regions within the regions of relatively vigorous response versus areas

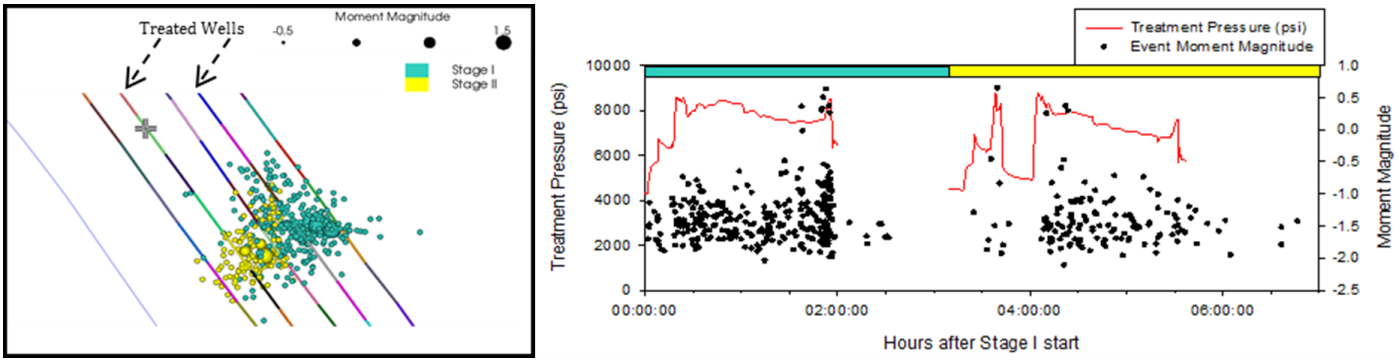

Figure 6. The events associated with two stages where larger events are recorded are shown in plan view (left) and against the treatment pressure with magnitude (right) against time.

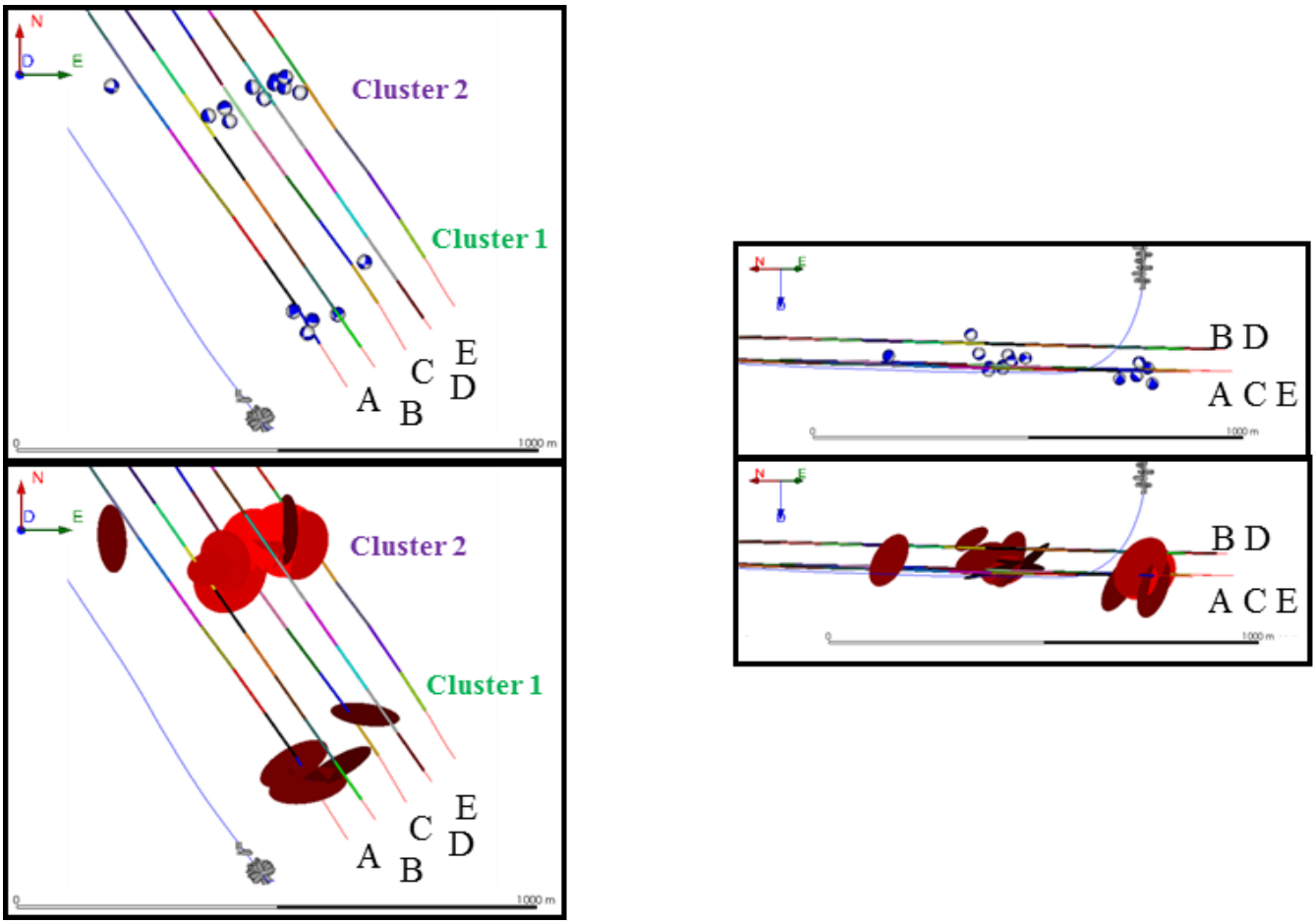

Figure 7. Plan views (left) and depth views (right) for the beachballs (above) and the discrete fracture network (below) of the events that qualify for moment tensor inversion from the two main clusters of large events over the completion.

within the array's detectability radius of less effective response. The higher magnitude events seen on the near-surface array are in general associated with the areas of increased activity. These events are associated with higher-pressure intervals in the treatment programs, and in some cases preceding the largest pressures indicating that these larger events are representing slipping of larger pre-existing structures in response to the injection program.

In figure 5, we show a pie chart illustrating the difference that the accurate characterization of these higher-magnitude events has on the overall estimates of the radiated seismic energy. Considering only the 28 events recorded on the surface stations, these events comprise 83% of the seismic energy release of the treatment. The balance of the 4500 events only seen on the downhole array consists of 17% of the energy release. In terms of the surface area of fractures activated in the treatment, amongst the events detected

these events liberate an additional 4% of surface area. However, the additional surface area activated in the stages where these events are most prominent can range up to 27%.

The treatment pressure for two of these stages is plotted in figure 6, against the magnitudes of the events. The occurrence of these larger magnitude events appears to coincide with the highest treatment pressures. The implication of the timing indicates that the injection is driving failures of larger structures in the formation. It also identifies the importance of full bandwidth monitoring as no direct relationship between magnitude and pressure would have been seen by only considering the events as detected downhole (M< -1).

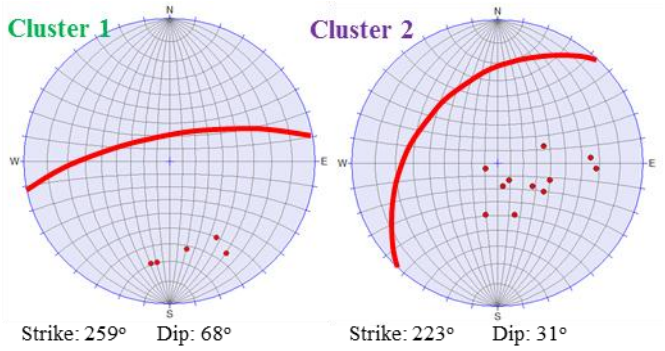

Figure 8. Lower stereographic projection for the poles to the fracture planes determined form the moment tensors for cluster 1 (left) and cluster 2 (right). The central fracture plane for each cluster is also shown.

5. MOMENT TENSOR INVERSION

Conventional recording of microseismic data with single arrays (such as the single array deployed downhole for this dataset) does not lend itself amenable to inversion for the source mechanism from the first motions of the wavefield. However, because a number of the larger magnitude events are recorded from a number of differing azimuths, there is enough sampling of the P, SV and SH wavefields to determine the moment tensors for these events. The events were solved by imposing a double-couple constraint on the inversion via a method of back-projecting the first motions of these waves back to the focal sphere [6]. In figure 7, we show the events as beachballs (top) in plan and depth view (left and right side of image, respectively) and as a discrete fracture network (bottom). These events are grouped into two clusters: cluster A occurs earlier near the toes of the treatment wells while cluster B occurs further up the treatment wells and few days later. While there is a well-known degeneracy in reconstructing the fracture orientation of a double-couple mechanism due to the equal admissibility of the two orthogonal nodal planes as solutions, we can assume that each cluster is responding to a similar state of stress spatially and use the ensemble of mechanisms to indicate which of the two candidate fracture planes is most consistent within the group. More specifically, within each cluster, we invert for the best-fitting orientations of the stress axes [7] and then can determine for each event, given that state of stress, which fracture plane is more likely.

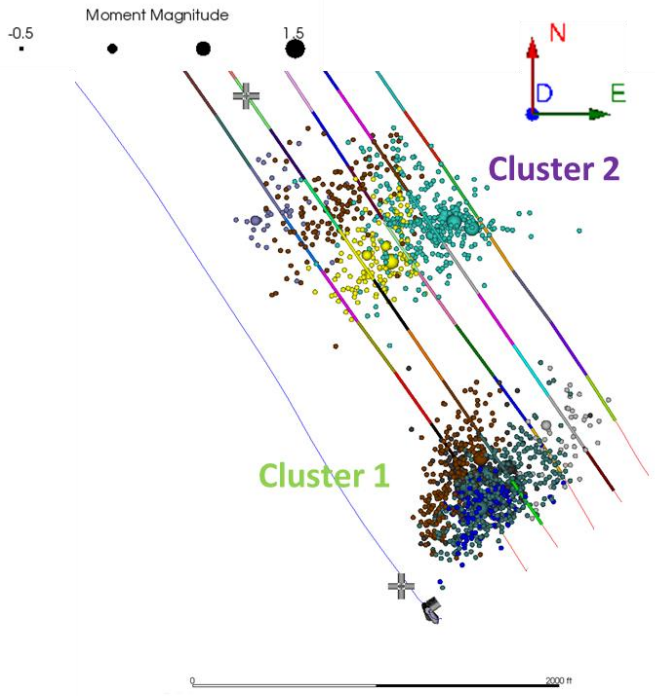

Figure 9. The event distributions for the stages associated with the larger events recorded on the near surface network.

In figure 8, we show the poles to the individual fracture planes, as well as the plane for the central orientation, for each cluster. We observe between the cluster A and cluster B events a shift in the fracture orientations: in cluster A the fractures concentrate around orientations striking N259°E and dipping 68°; for cluster B there is a broader spread of orientations but the fracture planes center around orientations striking N223°E and dipping more gently around 31°. The difference in fracture behavior may suggest a difference in the distribution of the fractures associated with the different clusters.

The difference in fracture orientations between the two clusters indicates a rotation of the stress regime. In figure 9, we show the event distributions for the stages associated with the larger events seen on the surface. The overall trends of the stages undergoes a rotation between the two clusters indicating that there does seem to be an overall stress rotation over the few days between cluster 1 and 2. The implication of this apparent perturbation to the local stress regime is that the larger events may be accommodating a Columbic stress perturbation.

6. CONCLUSIONS

In this paper, we have detailed the utility of augmenting the usual downhole microseismic monitoring arrays of high frequency geophones with a modest network of lower frequency sensors deployed at the surface. The faithful recording of these lower frequencies allows for accurate characterization of the higher magnitude events. Where the first motions of the events are observed from a wide azimuthal distribution of stations on the surface, the mechanisms and underlying fracture orientations may be determined.

In the case study we consider, 28 events of the over 4500 event recorded by the downhole array over the course of the multi well completion are observed form the surface array. This small minority of the total event count encompasses over 80% of the total recorded seismic energy radiated and a further 11,870 m^2 of activated fracture surface area in this treatment. These events are tied to the injection through their apparent response to treatment pressure increases suggesting that pre-existing fractures and faults are being activated. The events occur in two clusters separated by a few days over the treatment and the fracture sets seem to show a rotation to more shallowly dipping orientations from the first to second clusters indicating a rotation of the stress regime that may be mirrored in the rotation observed in the event trends between the two stages. Overall, the identification of the actual discrete fracture network over many size scales by utilizing a hybrid monitoring approach allows for a better understanding of the fracturing processes associated with stimulations.

1. Hanks, T. and H. Kanamori. 1979. A Moment Magnitude Scale. *J. of Geophys. Res.*, 84: 2348-2350.
2. Baig, A. M. and T. I. Urbancic. 2010. Magnitude Determination, Event Detectability, and Assessing the Effectiveness of Microseismic Monitoring Programs in Petroleum Applications. *CSEG Recorder*, 35: 22-26.
3. Brune, J. 1970. Tectonic stress and seismic shear waves from earthquakes. *J. of Geophys. Res.*, 75: 4997-5009.
4. Boatwright, J. 1980. A spectral theory for circular seismic sources: simple estimates of source duration, dynamic stress drop, and radiated energy. *Bull. of the Seism. Soc. of Am.*, 70: 1-28.
5. Reine, C. A. and R. B. Dunphy. 2011. Weighing in on the Seismic Scale: The use of Seismic Fault Measurements for Constructing Discrete Fracture Networks in the Horn River Basin. In *Proceedings of the 2011 CSPG CSEG CWLS Convention, Calgary, May 9-11, 2011*.
6. Trifu, C-I., D. Angus, and V. Shumila, 2000. A fast evaluation of the seismic moment tensor for induced seismicity, *Bull. of the Seism. Soc. of Am.*, 90: 1521–1527.
7. Gephart, J. and D. Forsyth. 1984. An improved method for determining the regional stress tensor using earthquake focal mechanism data: An application to the San Fernando earthquake sequence. *J. of Geophys. Res.*, 89: 9305–9320.